We are IntechOpen,
the world's leading publisher of
Open Access books
Built by scientists, for scientists

4,800
Open access books available

122,000
International authors and editors

135M
Downloads

Our authors are among the

154
Countries delivered to

TOP 1%
most cited scientists

12.2%
Contributors from top 500 universities

CLARIVATE ANALYTICS
**BOOK
CITATION
INDEX**
INDEXED

WEB OF SCIENCE™

Selection of our books indexed in the Book Citation Index
in Web of Science™ Core Collection (BKCI)

Interested in publishing with us?
Contact book.department@intechopen.com

Numbers displayed above are based on latest data collected.
For more information visit www.intechopen.com

Electronic Band Structure of Carbon Nanotubes in Equilibrium and None-Equilibrium Regimes

Mehdi Pakkhesal and Rahim Ghayour
Department of Electrical Engineering,
School of Engineering,
Shiraz University, Shiraz,
Iran

1. Introduction

The exploration of CNTs was a great contribution to the world of science and technology. After its exploration in 1991 by Iijima [1], extensive practical and theoretical researches about its nature gradually began to develop [2-6]. Today, we know about CNTs much more about its chemical, mechanical, optical and electrical properties than before. The methods of fabrication have also progressed. Due to their electrical and optical properties, CNTs are the subject of studies about their usage in new electronic and optoelectronic devices. In this chapter we will focus on their electronic band structure, because it is the most important characteristic of a solid that should be studied to be used in determination of its electronic, optical and optoelectronic properties. In order to investigate the electronic band structure of a solid, it is first necessary to have a good understanding of its crystal lattice and atomic structure. Therefore, as the first step of this chapter we will begin with the investigation of the geometry of SWCNTs. Then we will continue with the calculation of allowed wave vectors for the electronic transport. Having finished this step, we will introduce the electronic band structure of SWCNTs.

As is known, single walled carbon nanotube or SWCNT consists of grephene sheet that is rolled into a cylinder over a vector called "chiral vector" (Fig. 1(a)) so that the beginning and the end of this vector join to form the circumstantial circle of the cylinder Fig. 1(b).

As is shown in Fig. 1(a) the chiral vector may be written in terms of unit vectors $\mathbf{a}_1$ and $\mathbf{a}_2$, therefore $\mathbf{C}$ may be written as:

$$\mathbf{C} = m\mathbf{a}_1 + n\mathbf{a}_2 \tag{1}$$

Here $|\mathbf{a}_1| = |\mathbf{a}_2| = a_0 = \sqrt{3}a_{\text{C-C}}$ where $a_{\text{C-C}}$ is the bonding distance of the two adjacent carbon atom and is equal to 0.142nm and m > n. Having been familiar with chiral vector, its usage and its relationship with unit vectors $\mathbf{a}_1$ and $\mathbf{a}_2$, one can investigate the geometry of carbon nanotube.
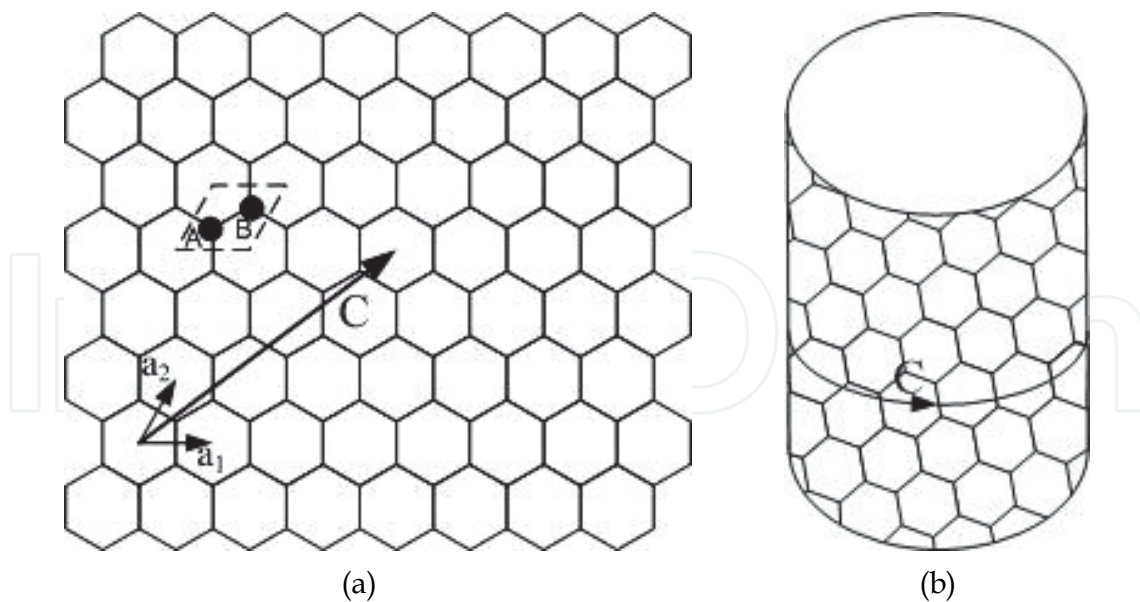
Fig. 1. (a) Illustration of Chiral vector **C** and unit vectors a_1 and a_2, A and B the two lattice sites of the graphene lattice. (b) The graphene sheet when rolled over Chiral vector **C.**

2. Investigation of the geometry of SWCNT

2.1 The investigation of radius and the chiral angle

In this section of this chapter we continue with the calculation of some aspects of the geometry of SWCNT, e.g. radius, chiral angle. As is illustrated in Fig. 1(b), the chiral vector **C** coincides the circumference of the cross sectional circle of the cylinder. Now, keeping this reality in the mind, we can easily infer the radius of the cylinder:

$$|\mathbf{C}| = 2\pi r \tag{2a}$$

which yields:

$$r = \frac{a_{C-C}}{2\pi}\sqrt{3\left(m^2 + n^2 + mn\right)} \tag{2b}$$

Next, we are to investigate a quantity called chiral angle. Chiral angle is the angle between chiral vector and the unit vector $\mathbf{a}_1$. The value can simply be calculated as:

$$\theta = \tan^{-1}\left(\frac{\sqrt{3}n}{2m+n}\right) \tag{3}$$

This value is a symbol of the way that the carbon atomic pairs (unit cell of graphene) are arranged.

2.2 Translational, helical and rotational symmetries

In this section we explain the three major types of symmetries of SWCNT. As a chiral structure, SWCNT is expected to have a *translational* symmetry. Thus, if we represent this symmetry with the vector **T**, such that **T** = $t_1\mathbf{a}_1 + t_2\mathbf{a}_2$ (t_1 and t_2 are natural numbers) we are faced with shortest symmetry vector that is perpendicular to the vector **C**, so:

$$\mathbf{C}.\mathbf{T} = 0 \tag{4}$$

Therefore:

$$(t_1\mathbf{a_1} + t_2\mathbf{a_2}).(\ m\mathbf{a_1} + n\mathbf{a_2}) = 0 \tag{5}$$

in solving this equation we note that $\mathbf{a}_i.\mathbf{a}_j$ is equal to $0.5a_0^2$ if $i \neq j$ and is equal to a_0^2 if $i = j$. Now, solving (5), regarding that p_1, p_2, m and n are positive natural numbers, $m > n$ and we are seeking for the smallest value of p_1 and p_2, we will have the following equation:

$$\frac{t_2}{t_1} = \frac{-\dfrac{2n+m}{\gcd(2n+m,2m+n)}}{\dfrac{2m+n}{\gcd(2n+m,2m+n)}} \tag{6}$$

$$\mathbf{T} = -\frac{2n+m}{\gcd(2n+m,2m+n)}\mathbf{a}_1 + \frac{2m+n}{\gcd(2n+m,2m+n)}\mathbf{a}_2 \tag{7}$$

where gcd is standing for Greatest Common Devisor. As described before, $\mathbf{T}$ is a translational symmetry vector which means that if we move on the surface of the nanotube by $\mathbf{T}$ vector we catch up similar points.

Now we are to investigate the second and the third types of symmetries on the surface of the SWCNT which are *helical* and *rotational* symmetries [7]. As mentioned before, nanotube's cylinder is formed by rolling graphene on the lattice vector $\mathbf{C}$. Thus, we begin our investigation by means of a mapping process. We first, try to map the unit cell of graphene on the surface of the cylinder. We suppose that $\mathbf{d}$ is a vector such that it begins from the lattice site A and ends to lattice site B. The first atom can be placed on an arbitrary place on the surface of the cylinder. The second atom must be placed at the height of $\dfrac{|\mathbf{d} \times \mathbf{C}|}{|\mathbf{C}|}$ from the first atom and the azimuthal angle of $2\pi \dfrac{|\mathbf{d}.\mathbf{C}|}{|\mathbf{C}|^2}$ with respect to the first atom. Until now, we have mapped a unit cell of graphene to the surface the cylinder. Where to place the next atomic pair? Now, we want to find a slice of the cylinder such that it includes the minimum number of graphene unit cells. We know that, the area of this slice is calculated using the formula: $A_M = 2\pi r h$. Where h is the height of the mentioned section. h can be regarded as the magnitude of a vector $\mathbf{H} = p_1\mathbf{a_1} + p_2\mathbf{a_2}$; therefore, A_M can be expressed as:

$$A_M = |\mathbf{H} \times \mathbf{B}| = (p_1 m - p_2 n)|\mathbf{a_1} \times \mathbf{a_2}| \tag{8}$$

Now we are to minimize the term: p_1m-p_2n. Mathematically, it can be shown that this term is minimized when:

$$p_1 m - p_2 n = \pm N \tag{9}$$

where $N = gcd(m,n)$. In order to acquire unique values for p_1 and p_2 we find p_1 and p_2 such that $p_1 \geq 0$ and $|\mathbf{H}|$ has the minimum value. Knowing that the area of a unit cell of the

graphene (which is an atomic pair) is equal to $\left| \mathbf{a_1} \times \mathbf{a_2} \right|$, the mentioned slice contains N atomic pairs which are located in the multiples of the azimuthal angle of $\dfrac{2\pi}{N}$. This implies a symmetry in azimuthal direction which is so called "rotational symmetry". Now, we return to our question which is finding the place of the second atomic pair on the surface of the tubule. After finding the **H** vector with the mentioned conditions, it is clear that it implies a type of symmetry in the helical direction (along the vector **H**) [7]. There for, the second atomic pair should be place at a position which is located by an **H** vector next to the first atomic pair. The third atomic pair is located 2**H** from the first one and so on. This "helical motif" should be copied N times in angular space of $\dfrac{2\pi}{N}$ to construct whole the nanotube's structure. Now that we have known the symmetries of the nanotube, we are ready to investigate the band structure of SWCNT.

Fig. 2. In this figure the "helical motif" and **H** vector are illustrated.

3. The band structure of SWCNT in equilibrium conditions

3.1 Bloch function

At this step we are facing the problem of finding the wave function for a crystal lattice. In this situation we are facing periodic boundary conditions. Therefore, it is expected that we acquire a periodic wave function. Using these facts, in 1927 Bloch showed that the electron wave function has the following form for a crystal lattice:

$$\psi_{\mathbf{k}}(\mathbf{r}) = u_{\mathbf{k}}(\mathbf{r})e^{i\mathbf{k}\cdot\mathbf{r}} \tag{10}$$

where $\psi_{\mathbf{k}}(\mathbf{r})$ is the electron wave function, $u_{\mathbf{k}}(\mathbf{r})$ a periodic function with the period of the crystal and **k** is the electron wave vector. After this step, we find the energy of the electron, E, using the Hamiltonian operator, H, as follows:

$$H\psi_{\mathbf{k}}(\mathbf{r}) = E\psi_{\mathbf{k}}(\mathbf{r}) \tag{11}$$

But we don't have $u_k(\mathbf{r})$. Therefore, we don't know the exact form of $\psi_k(\mathbf{r})$. There are a variety of methods to describe the interaction of electron and the crystal lattice. In this chapter we investigate the mentioned interaction according to nearest neighbor π-Tight Binding (π-TB) and the third neighbor π-TB method.

3.2 Brillouin zone

Suppose that we have a wave function of the form $e^{i\mathbf{G}\cdot\mathbf{r}}$. We want to find $\mathbf{G}$ vector such that

$$e^{i\mathbf{G}\cdot(\mathbf{r}+\mathbf{R})} = e^{i\mathbf{G}\cdot\mathbf{r}} \tag{12}$$

or:

$$\mathbf{G}\cdot\mathbf{R} = 2\pi l \tag{13}$$

where l is an arbitrary integer. Now regarding the following equations for $\mathbf{G}$ and $\mathbf{R}$:

$$\mathbf{G} = g_1\hat{\mathbf{k}}_1 + g_2\hat{\mathbf{k}}_2 + g_3\hat{\mathbf{k}}_3 \tag{14a}$$

$$\mathbf{R} = n_1\hat{\mathbf{a}}_1 + n_2\hat{\mathbf{a}}_2 + n_3\hat{\mathbf{a}}_3 \tag{14b}$$

where $\hat{\mathbf{a}}_1$, $\hat{\mathbf{a}}_2$, $\hat{\mathbf{a}}_3$ are unit vectors in lattice space and $\hat{\mathbf{k}}_1$, $\hat{\mathbf{k}}_2$, $\hat{\mathbf{k}}_3$ are unit vectors in, so called, "reciprocal lattice" space. If we apply (13) we will have:

$$\mathbf{G}\cdot\mathbf{R} = 2\pi\left(n_1g_1 + n_2g_2 + n_3g_3\right) \tag{15}$$

which suggests that:

$$\begin{array}{ccc} \hat{\mathbf{k}}_1\cdot\hat{\mathbf{a}}_1 = 2\pi & \hat{\mathbf{k}}_1\cdot\hat{\mathbf{a}}_2 = 0 & \hat{\mathbf{k}}_1\cdot\hat{\mathbf{a}}_3 = 0 \\ \hat{\mathbf{k}}_2\cdot\hat{\mathbf{a}}_1 = 0 & \hat{\mathbf{k}}_2\cdot\hat{\mathbf{a}}_2 = 2\pi & \hat{\mathbf{k}}_2\cdot\hat{\mathbf{a}}_1 = 0 \\ \hat{\mathbf{k}}_3\cdot\hat{\mathbf{a}}_1 = 0 & \hat{\mathbf{k}}_3\cdot\hat{\mathbf{a}}_2 = 0 & \hat{\mathbf{k}}_3\cdot\hat{\mathbf{a}}_3 = 2\pi \end{array} \tag{16}$$

Solving above equations [8]:

$$\hat{\mathbf{k}}_1 = 2\pi\frac{\hat{\mathbf{a}}_1 \times \hat{\mathbf{a}}_3}{\hat{\mathbf{a}}_1\cdot\left(\hat{\mathbf{a}}_2 \times \hat{\mathbf{a}}_3\right)} \tag{17a}$$

$$\hat{\mathbf{k}}_2 = 2\pi\frac{\hat{\mathbf{a}}_3 \times \hat{\mathbf{a}}_1}{\hat{\mathbf{a}}_1\cdot\left(\hat{\mathbf{a}}_2 \times \hat{\mathbf{a}}_3\right)} \tag{17b}$$

$$\hat{\mathbf{k}}_3 = 2\pi\frac{\hat{\mathbf{a}}_1 \times \hat{\mathbf{a}}_2}{\hat{\mathbf{a}}_1\cdot\left(\hat{\mathbf{a}}_2 \times \hat{\mathbf{a}}_3\right)} \tag{17c}$$

Now we have unit vectors of the reciprocal lattice. In order to get the Brillouin zone we should we should apply the following condition:

$$\left(\mathbf{k} - \mathbf{G}\right)^2 = \mathbf{k}^2 \tag{18a}$$

or:

$$\mathbf{k.G} = \frac{1}{2}\mathbf{G}^2 \qquad (18b)$$

thus:

$$\mathbf{k} = \frac{1}{2}\mathbf{G} \qquad (18c)$$

Using (18-c) we can draw the borders of the Brillouin zone. The inner most area is called the first Brillouin zone and hence, simply it is called "Brillouin zone".

Now we return to our lattice which is graphene sheet, a two dimensional crystal. If we write (16) for this kind of lattice we will have:

$$\begin{array}{ll} \mathbf{k_1.a_1} = 2\pi & \mathbf{k_1.a_2} = 0 \\ \mathbf{k_2.a_1} = 0 & \mathbf{k_2.a_2} = 2\pi \end{array} \qquad (19)$$

From (19) it is clear that $\mathbf{k_1}$ and $\mathbf{k_2}$ are perpendicular to $\mathbf{a_2}$ and $\mathbf{a_1}$ respectively. Having $\mathbf{a_1}$ and $\mathbf{a_2}$ from Fig. 1(a) we can easily find $\mathbf{k_1}$ and $\mathbf{k_2}$ and draw the Brillouin zone (Fig. 3).
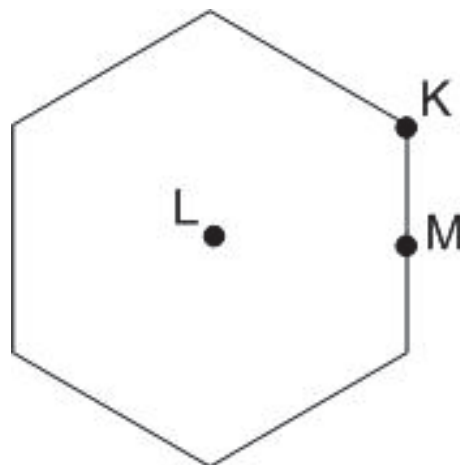

Fig. 3. The Brillouin zone for the graphene lattice is illustrated. L, K and M are high symmetry points.

As mentioned earlier, theoretically, SWCNT can be considered as a graphene lattice that is rolled over into a cylinder. Thus, according to Fig. 1(b) we catch up the following:

$$u_{\mathbf{k}}(\mathbf{r})e^{i\mathbf{k.(r+C)}} = u_{\mathbf{k}}(\mathbf{r})e^{i\mathbf{k.r}} \qquad (20)$$

Therefore [9]:

$$\mathbf{k.C} = 2\pi l \qquad (21)$$

where l is again, an arbitrary integer. This boundary condition which is so called, "Born-von Karman" condition, makes the Brillouin zone to be quantized. Fig. 4 shows this fact. At this point we can begin our investigation about the band structure of SWCNT.
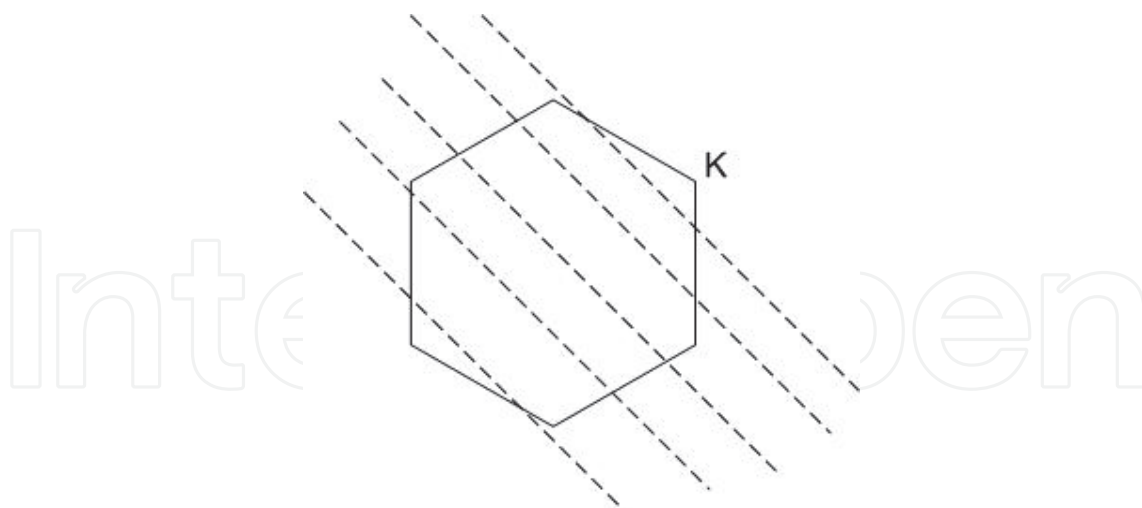
Fig. 4. The Born-von Karman condition makes the SWCNT's Brillouin zone to be quantized.

3.3 Tight-binding approximation

As mentioned, there are many methods and approximations that are used to investigate the electronic band structure of a solid. In this section we use the tight-binding approximation. In this approximation we consider the wave function of an electron as the Linear Combination of Atomic Orbitals and hence the method is also called as LCAO.

As is known, the energy of an electron can be estimated using Schrödinger's equation as follows:

$$\left[-\frac{\hbar^2 \nabla^2}{2m} + V(\mathbf{r}) \right] \psi_{\mathbf{k}}(\mathbf{r}) = E \psi_{\mathbf{k}}(\mathbf{r}) \tag{22}$$

where m is the mass of an electron and $\psi_{\mathbf{k}}(\mathbf{r})$ is the wave function of a single electron with the wave vector $\mathbf{k}$. Now $\psi_{\mathbf{k}}(\mathbf{r})$ is written as the following:

$$\psi_{\mathbf{k}}(\mathbf{r}) = \sum_{\mathbf{r}} c_{\mathbf{kr}} \varphi_{\mathbf{kr}}(\mathbf{r}) \tag{23}$$

where $\varphi_{\mathbf{kr}}(\mathbf{r})$'s are basis functions that are made from atomic orbitals as:

$$\varphi_{\mathbf{kr}}(\mathbf{r}) = \frac{1}{\sqrt{N_t}} \sum_{\substack{unit\,cells\,of \\ the\,system}} e^{i\mathbf{k}.\mathbf{R}} \chi_{\mathbf{r}}(\mathbf{R} - \mathbf{r}) \tag{24}$$

where N_t is the total number of unit cells in the system. We regard the single $2p_z$ orbital of the carbon atoms to used in (23); besides, we take into account the interaction of the nearest neighbor atoms (Fig. 5), because they have the most important role in formation of the energy states [10]. We write the wave function $|\psi\rangle$ in terms of basis functions, $|\varphi_1\rangle$ and $|\varphi_2\rangle$ as the following:

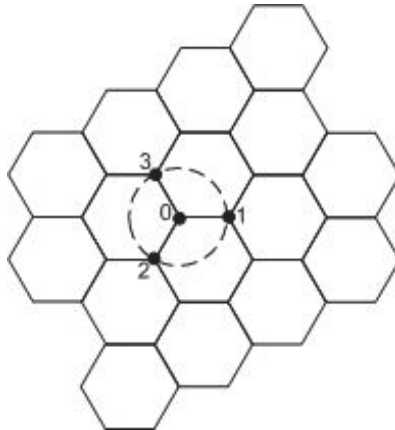$$|\psi\rangle = c_1 |\varphi_1\rangle + c_2 |\varphi_2\rangle \tag{25}$$

Fig. 5. In this figure the nearest neighbor atoms with respect to atom 0 are illustrated.

$|\varphi_1\rangle$ corresponds to atom 0 and $|\varphi_2\rangle$ corresponds to atoms 1, 2 and 3 in Fig. 5. Now applying (22) to (25) yields:

$$H|\psi\rangle = c_1 H|\varphi_1\rangle + c_2 H|\varphi_2\rangle = c_1 E|\varphi_1\rangle + c_2 E|\varphi_2\rangle \tag{26}$$

and consequently:

$$c_1\langle\varphi_1|H|\varphi_1\rangle + c_2\langle\varphi_1|H|\varphi_2\rangle = c_1 E\langle\varphi_1|\varphi_1\rangle + c_2 E\langle\varphi_1|\varphi_2\rangle \tag{27a}$$

$$c_1\langle\varphi_2|H|\varphi_1\rangle + c_2\langle\varphi_2|H|\varphi_2\rangle = c_1 E\langle\varphi_2|\varphi_1\rangle + c_2 E\langle\varphi_2|\varphi_2\rangle \tag{27b}$$

Now, we define the following values:

$$H_{AA} = \langle\varphi_1|H|\varphi_1\rangle \tag{28a}$$

$$H_{AB} = \langle\varphi_1|H|\varphi_2\rangle \tag{28b}$$

$$S_{AA} = \langle\varphi_1|\varphi_1\rangle \tag{28c}$$

$$S_{AB} = \langle\varphi_1|\varphi_2\rangle \tag{28d}$$

then (27-a) becomes:

$$c_1(H_{AA} - ES_{AA}) + c_2(H_{AB} - ES_{AB}) = 0 \tag{29}$$

knowing that:

$$|\varphi_1\rangle = \frac{1}{\sqrt{N_t}} \sum_{Lattice\,site\,A} e^{i\mathbf{k}.\mathbf{R}_A} \chi_\mathbf{r}(\mathbf{r}-\mathbf{R}_A) \tag{30a}$$

$$|\varphi_2\rangle = \frac{1}{\sqrt{N_t}} \sum_{Lattice\,site\,B} e^{i\mathbf{k}.\mathbf{R}_B} \chi_\mathbf{r}(\mathbf{r}-\mathbf{R}_B) \tag{30b}$$

Replacing (30-a) and (30-b) in (28-a) to (28-d) yields:

$$H_{AA} = \varepsilon_{2p} \tag{31a}$$

$$H_{AB} = (e^{i\mathbf{k}.\mathbf{R}_{11}} + e^{i\mathbf{k}.\mathbf{R}_{12}} + e^{i\mathbf{k}.\mathbf{R}_{13}})V_{pp\pi} \tag{31b}$$

$$S_{AA} = 1 \tag{31c}$$

$$S_{AB} = (e^{i\mathbf{k}.\mathbf{R}_{11}} + e^{i\mathbf{k}.\mathbf{R}_{12}} + e^{i\mathbf{k}.\mathbf{R}_{13}})s_0 \tag{31d}$$

$$H_{BB} = \langle \varphi_2 | H | \varphi_2 \rangle = H_{AA} \tag{31e}$$

$$H_{BA} = \langle \varphi_2 | H | \varphi_1 \rangle = H_{AB}^* \tag{31f}$$

$$S_{BB} = S_{AA} = 1 \tag{31g}$$

$$S_{BA} = S_{AB}^* \tag{31h}$$

which make (27-b) to become:

$$c_1(H_{AB}^* - ES_{AB}^*) + c_2(H_{AA} - ES_{AA}) = 0 \tag{32}$$

considering (29) and (32) together; to have a non trivial solutions for c_1 and c_2 we should have:

$$\begin{vmatrix} H_{AA} - ES_{AA} & H_{AB} - ES_{AB} \\ H_{AB}^* - ES_{AB}^* & H_{AA} - ES_{AA} \end{vmatrix} = 0 \tag{33}$$

Solving (33) for E [11]:

$$E(\mathbf{k})^{\pm} = \frac{-(-2E_0 + E_1) \pm \sqrt{(-2E_0 + E_1)^2 - 4E_2E_3}}{2E_3} \tag{34}$$

where:

$$E_0 = H_{AA}S_{AA} \tag{35a}$$

$$E_1 = S_{AB}H_{AB}^* + H_{AB}S_{AB}^* \tag{35b}$$

$$E_2 = H_{AA}^2 - H_{AB}H_{AB}^* \tag{35c}$$

$$E_3 = S_{AA}^2 - S_{AB}S_{AB}^* \tag{35d}$$

Neglecting the overlap of 2p$_z$ orbitals of atomic neighbors, S_{AB}, we get:

$$E(\mathbf{k})^{\pm} = \pm V_{pp\pi}\sqrt{3 + 2\cos(\mathbf{k}.\mathbf{a}_1) + 2\cos(\mathbf{k}.\mathbf{a}_2) + 2\cos(\mathbf{k}.(\mathbf{a}_1 - \mathbf{a}_2))} \tag{36}$$

Now applying Born von-Karman boundary condition (equation (21)) to (36) one can draw the energy diagram or the electronic band structure of SWCNT. Illustrated in Fig. 6(a) to 6(f) are the electronic band structures for several chiral vectors. At this step of our work, it is necessary to mention a few points. First of all, according to their chiralities, SWCNTs are

(a)   (b)

(c)   (d)

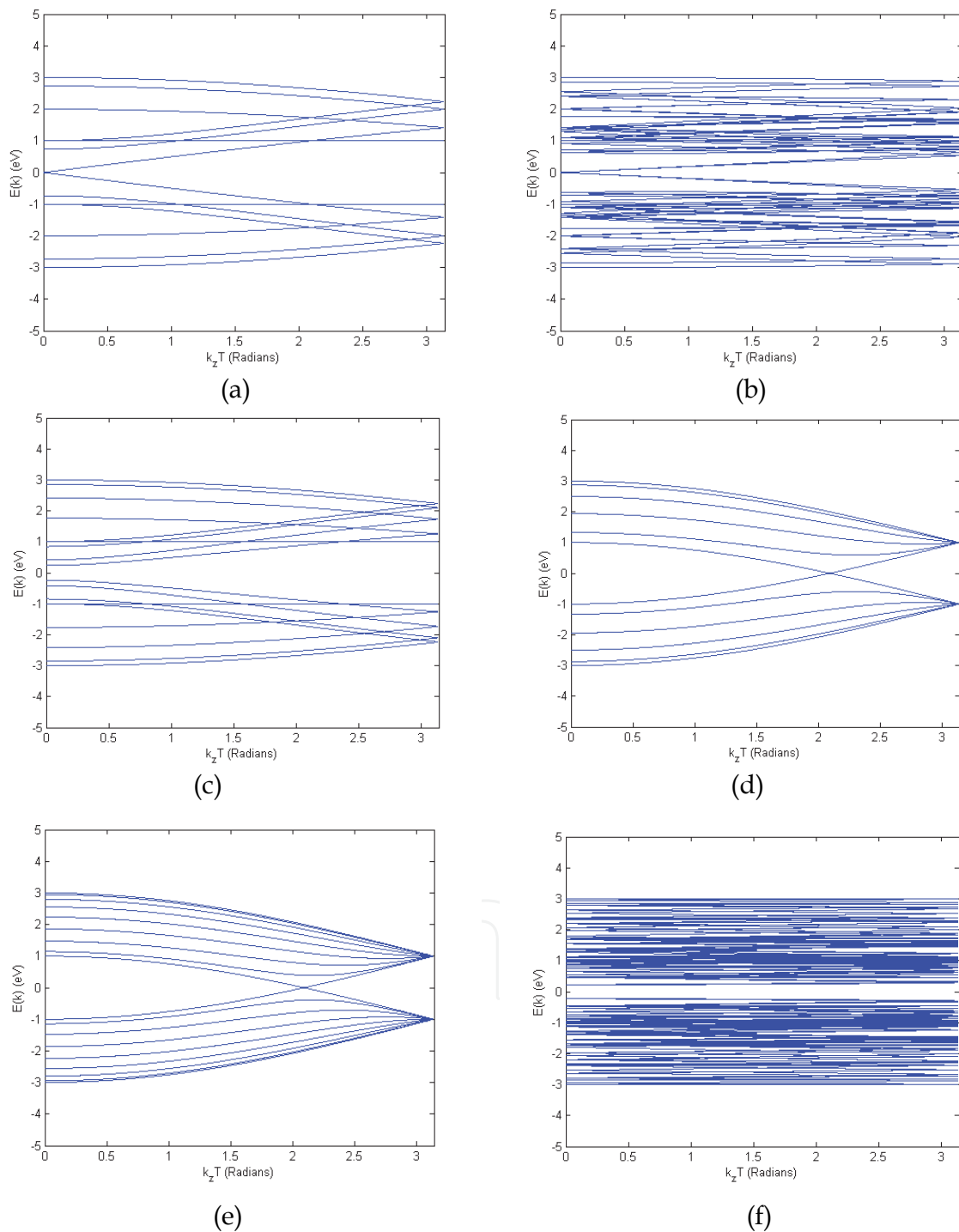(e)   (f)

Fig. 6. The electronic band structures of several nanotubes according to (36) are illustrated. (a) is the electronic band structure of chiral vector (6,0), (b) (6,3), (c) (8,0), (d) (5,5), (e) (8,8), (f) (5,4)

roughly divided to three classifications. A nanotube with chirality of (n,0) is called a "zig-zag" nanotube. A nanotube with chirality of (n,n) is called an "armchair" nanotube and a nanotube without the two mentioned chiralities, is called a "chiral" nanotube. As examples, illustrated in Fig. 6(a) and (c) are the band structure of SWCNTs with chiral vectors (6,0) and (8,0) which are zig-zag nanotubes, and Fig. 6(d) and (e) show the band structure of SWCNTs with chiral vectors (5,5) and (8,8) which are armchair nanotubes.

As the Second point, it worth noting that, if we examine (36) with Born-von Karman boundary condition, it is observed that for any chiral vector (n,m) when (n-m) mod 3 is equal to 0, then the band-gap is equal to zero. Two samples of this type are shown in Fig. 6(a) and (b). It is clear that according to this model armchair nanotubes are of this type. At early days it was believed that these nanotubes are metallic, but next, the deeper researches and calculations with other methods and approximations showed that they are "semi-metallic"[12].

Until now, we have performed our analytic calculations with the two assumptions. First, we assumed that the overlap of the two nearest neighbors is zero. Second, we assumed that the $2p_z$ orbitals of the second and the third neighbors have no participation in formation of the band structure. However, in the following lines, we take into account the donation of these neighbors to the formation of the band structure of SWCNT.

Shown in Fig. 7 are the second and the third neighbors of the atom 0 of this figure. According to this figure, one can write:

$$\mathbf{R_{11}} - \mathbf{R_0} = \frac{2\mathbf{a_1} - \mathbf{a_2}}{3} \tag{37a}$$

$$\mathbf{R_{12}} - \mathbf{R_0} = \frac{2\mathbf{a_2} - \mathbf{a_1}}{3} \tag{37b}$$

$$\mathbf{R_{13}} - \mathbf{R_0} = -\frac{\mathbf{a_1} + \mathbf{a_2}}{3} \tag{37c}$$

$$\mathbf{R_{21}} - \mathbf{R_0} = \mathbf{a_1} - \mathbf{a_2} \tag{37d}$$

$$\mathbf{R_{22}} - \mathbf{R_0} = \mathbf{a_1} \tag{37e}$$

$$\mathbf{R_{23}} - \mathbf{R_0} = \mathbf{a_2} \tag{37f}$$

$$\mathbf{R_{24}} - \mathbf{R_0} = -(\mathbf{a_1} - \mathbf{a_2}) \tag{37g}$$

Now, if we apply the formalism of the tight-binding approach, we catch up the following formulae:

$$E_0 = [\varepsilon_{2p} + \gamma_1 u(\mathbf{k})][1 + s_1 u(\mathbf{k})] \tag{38a}$$

$$E_1 = 2s_0 s\gamma_0 f(\mathbf{k}) + (s_0\gamma_2 + s_2\gamma_0)g(\mathbf{k}) + 2s_2\gamma_2 f(2\mathbf{k}) \tag{38b}$$

$$E_2 = [\varepsilon_{2p} + \gamma_1 u(\mathbf{k})]^2 - \gamma_0^2 f(\mathbf{k}) - \gamma_0\gamma_2 g(\mathbf{k}) - \gamma_2^2 f(2\mathbf{k}) \tag{38c}$$

$$E_3 = [1+s_1u(\mathbf{k})]^2 - s_0{}^2f(\mathbf{k}) - s_0s_2g(\mathbf{k}) - s_2{}^2f(2\mathbf{k}) \tag{38d}$$

$$g(\mathbf{k}) = 2u(\mathbf{k}) + u(2k_1\text{-}k_2, k_1\text{-}2k_2) \tag{38e}$$

$$f(\mathbf{k}) = 3+u(\mathbf{k}) \tag{38f}$$

$$u(\mathbf{k}) = 2\cos(\mathbf{k}.\mathbf{a_1}) + 2\cos(\mathbf{k}.\mathbf{a_2}) + 2\cos(\mathbf{k}.(\mathbf{a_1} - \mathbf{a_2})) \tag{38g}$$

where the hopping parameters γ_0, γ_1, γ_2 and the overlap parameters s_0, s_1 and s_2 are introduced as follows:

$$\gamma_0 = \langle \chi(\mathbf{r} \text{-} \mathbf{R_0}) | H | \chi(\mathbf{r} \text{-} \mathbf{R_{1i}}) \rangle \tag{39a}$$

$$s_0 = \langle \chi(\mathbf{r} \text{-} \mathbf{R_0}) | \chi(\mathbf{r} \text{-} \mathbf{R_{1i}}) \rangle \tag{39b}$$

$$\gamma_1 = \langle \chi(\mathbf{r} \text{-} \mathbf{R_0}) | H | \chi(\mathbf{r} \text{-} \mathbf{R_{2i}}) \rangle \tag{39c}$$

$$s_1 = \langle \chi(\mathbf{r} \text{-} \mathbf{R_0}) | \chi(\mathbf{r} \text{-} \mathbf{R_{2i}}) \rangle \tag{39d}$$

$$\gamma_2 = \langle \chi(\mathbf{r} \text{-} \mathbf{R_0}) | H | \chi(\mathbf{r} \text{-} \mathbf{R_{3i}}) \rangle \tag{39e}$$

$$s_2 = \langle \chi(\mathbf{r} \text{-} \mathbf{R_0}) | \chi(\mathbf{r} \text{-} \mathbf{R_{3i}}) \rangle \tag{39f}$$

Then, (38-a) to (38-g) should be replaced in (34) to get the energy formula. The numerical values for γ_0, γ_1, γ_2 and s_0, s_1, s_2 in addition to a comparison between the results of the mentioned method with the nearest neighbor π-TB can be found in [13].
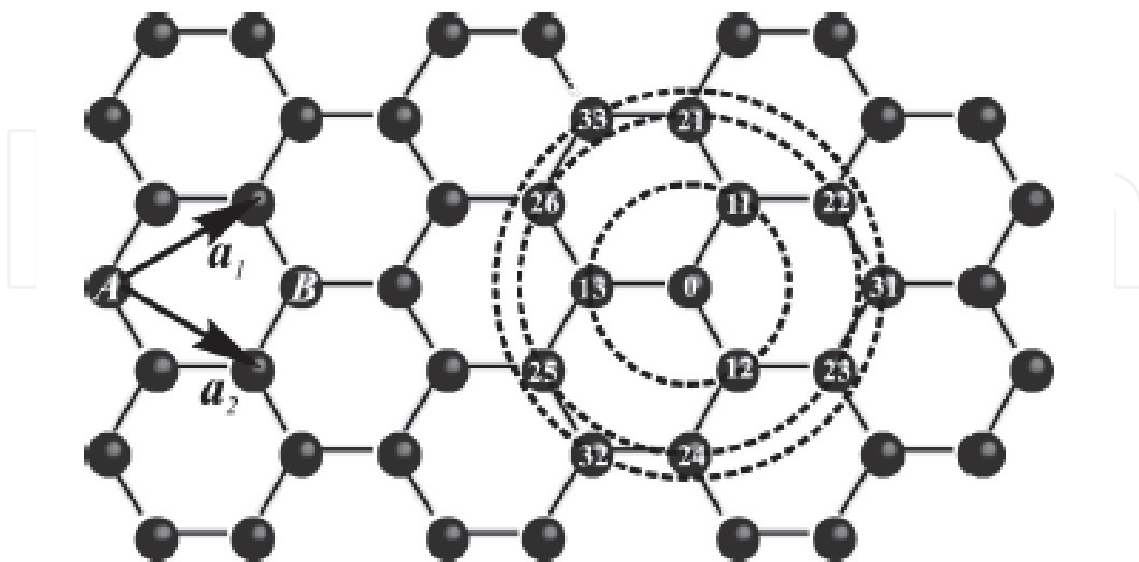

Fig. 7. In this figure the nearest neighboring atoms, the second and the third neighboring atoms are illustrated.

At this point, we continue our work by examining some SWCNTs with different chiral vectors to investigate the effect of radius and chiral angle on the band-gap of these nanotubes. In Table I we have collected chiral vectors that have the same radii but different chiral angles to investigate such an effect. In this table from left, the first column shows the pairs of chiral vectors with the same radii. The second column shows their radii; the third column, their chiral angle; the forth one, the difference between chiral angles; the fifth column indicates the energy gap and finally sixth column shows the difference in band-gap which emanates from the difference between the chiral angle of the nanotubes with the same radii. As can be seen in this table the effect radius on the band-gap is considerable and the band-gap is approximately proportional to $\frac{1}{R}$. On the other hand, as can be concluded from this table, change of the chiral angle has a little effect on the band-gap of SWCNT.

C:(m,n)	r (nm)	θ (Degrees)	|Δθ| (Degrees)	G (eV)	|ΔG| (eV)
(9,1)	0.373	5.20	21.78	1.091448	0.031806
(6,5)		26.99		1.059642	
(9,8)	0.576	28.05	17.89	0.694152	0.018414
(13,3)		10.15		0.675738	
(14,3)	0.615	9.51	13.17	0.655092	0.010044
(11,7)		22.68		0.645048	
(15,2)	0.630	6.17	9.43	0.617706	0.021204
(13,5)		15.60		0.63891	
(15,4)	0.679	11.51	15.17	0.593154	0.000558
(11,9)		26.69		0.593712	
(18,2)	0.746	5.20	21.78	0.5219532	0.0054126
(12,10)		26.99		0.5273658	
(19,2)	0.785	4.94	17.89	0.5116302	0.001953
(14,9)		22.84		0.5135832	
(19,3)	0.808	7.22	7.34	0.483786	0.01395
(17,6)		14.56		0.497736	
(19,5)	0.858	11.38	9.43	0.4684968	0.0026784
(16,9)		20.81		0.4658184	
(23,1)	0.920	2.11	21.78	0.4248612	0.01607
(16,11)		23.89		0.4409316	
(23,4)	0.987	7.88	16.42	0.3977982	0.014564
(17,12)		24.31		0.412362	
(29,4)	1.221	6.37	21.78	0.322524	0.019139
(19,17)		28.16		0.3416634	
(30,4)	1.260	6.17	9.43	0.3167766	0.0071982
(26,10)		15.60		0.3095784	

Table 1. A comparison between the effects of the radius and the chiral angle on the band-gap of SWCNT. In this table G is the band-gap. ΔG is the difference in band-gap of the two SWCNT with the different chiral angles.

4. The electronic band structure of SWCNTs under non-equilibrium conditions

4.1 The investigation of the band gap under mechanical strain

In this section of this chapter, we investigate the effect of the two types of mechanical strain, namely uniaxial (tensile) and torsional strains, by means of the two mentioned approximations.

If we denote the amount of uniaxial strain by σ_t, the angle of shear by α and the bonding lengthes $\mathbf{R_{11}}$-$\mathbf{R_0}$, $\mathbf{R_{12}}$-$\mathbf{R_0}$, $\mathbf{R_{13}}$-$\mathbf{R_0}$ by $\mathbf{r_1}$, $\mathbf{r_2}$ and $\mathbf{r_3}$ respectively, then, under these two type of strain we have the following relations [14]:

$$r_{it} \xrightarrow{\quad Tensile \quad} r_{it}(1+\sigma_t) \tag{40a}$$

$$r_{ic} \xrightarrow{\quad Torsion \quad} r_{ic} + r_{it}\tan(\alpha) \tag{40b}$$

where r_{it} is that part of $\mathbf{r_i}$ that is along the axis of the nanotube (with the unit vector $\hat{\mathbf{t}}$) and r_{ic} is that part of $\mathbf{r_i}$ that is in azimuthal direction or along the circumference of the nanotube (with the unit vector $\hat{\mathbf{c}}$). In order to use (40-a) and (40-b) we have to express (37) in terms of $\hat{\mathbf{t}}$ and $\hat{\mathbf{c}}$:

$$\mathbf{r_1} = \frac{an_1}{2d}\hat{\mathbf{c}} - \frac{1}{\sqrt{3}d}\left(n_2 + \frac{n_1}{2}\right)\hat{\mathbf{t}} \tag{41a}$$

$$\mathbf{r_2} = \frac{an_2}{2d}\hat{\mathbf{c}} + \frac{1}{\sqrt{3}d}\left(n_1 + \frac{n_2}{2}\right)\hat{\mathbf{t}} \tag{41b}$$

$$\mathbf{r_3} = -\left(\mathbf{r_1} + \mathbf{r_2}\right) \tag{41c}$$

Using these relations in conjunction with (40-a) and (40-b), we have the following formulae for $\mathbf{r_1}$, $\mathbf{r_2}$ and $\mathbf{r_3}$:

$$\mathbf{r_1} = \left[\frac{an_1}{2d} - \frac{\tan(\alpha)}{\sqrt{3}d}\left(n_2 + \frac{n_1}{2}\right)\right]\hat{\mathbf{c}} - \frac{(1+\sigma_t)}{\sqrt{3}d}\left(n_2 + \frac{n_1}{2}\right)\hat{\mathbf{t}} \tag{42a}$$

$$\mathbf{r_2} = \left[\frac{an_2}{2d} + \frac{\tan(\alpha)}{\sqrt{3}d}\left(n_1 + \frac{n_2}{2}\right)\right]\hat{\mathbf{c}} + \frac{(1+\sigma_t)}{\sqrt{3}d}\left(n_1 + \frac{n_2}{2}\right)\hat{\mathbf{t}} \tag{42b}$$

and (41-c) is still valid. At this step, we are to derive the 3rd neighbor π-tight-binding formulation to investigate the effect of uniaxial and torsional strains. We know that, there is the following formula for the interaction energy [14]:

$$\frac{\gamma_{0i}}{\gamma_0} = \frac{\langle \chi(\mathbf{r} - \mathbf{R_0}) | H | \chi(\mathbf{r} - \mathbf{R_{1i}}) \rangle \, with\,strain}{\langle \chi(\mathbf{r} - \mathbf{R_0}) | H | \chi(\mathbf{r} - \mathbf{R_{1i}}) \rangle \, without\,strain} = \left(\frac{a_{C-C}}{r_{1i}}\right)^2 \tag{43}$$

where a_{C-C} is the bond length in the absence of strain and r_{1i} with i =1,2,3 is $|\mathbf{r_i}|$ in the presence of strain. After performing the formal routine of the deriving of the tight-binding approximation formulae, we find:

$$E_0 = \left[\varepsilon_{2p} + \gamma_1 u(\mathbf{k}) \right]\left[1 + s_1 u(\mathbf{k}) \right] \tag{44a}$$

$$E_1 = f_{s\gamma}(\mathbf{k}) + \gamma_2 g_s(\mathbf{k}) + s_2 g_\gamma(\mathbf{k}) + 2s_2\gamma_2 f(\mathbf{k}) \tag{44b}$$

$$E_2 = \left[\varepsilon_{2p} + \gamma_1 u(\mathbf{k}) \right]^2 - f_{\gamma\gamma}(\mathbf{k}) - \gamma_2 g_\gamma(\mathbf{k}) - \gamma_2^2 f(2\mathbf{k}) \tag{44c}$$

$$E_3 = \left[1 + s_1 u(\mathbf{k}) \right]^2 - f_{ss}(\mathbf{k}) - s_2 g_s(\mathbf{k}) - s_2^2 f(2\mathbf{k}) \tag{44d}$$

where functions $f(\mathbf{k})$, $f_{s\gamma}(\mathbf{k})$, $g_s(\mathbf{k})$, $g_\gamma(\mathbf{k})$, $f_{\gamma\gamma}(\mathbf{k})$, and $f_{ss}(\mathbf{k})$ in addition to details of calculations are given in [15].

Now, it's time to apply (44-a) to (44-d) and see the results in comparison to other methods. Illustrated in Fig. 8 are the results of application of mentioned method for uniaxial and torsional strains in comparison with the nearest neighbor π-TB and the four orbital tight-binding approximations.
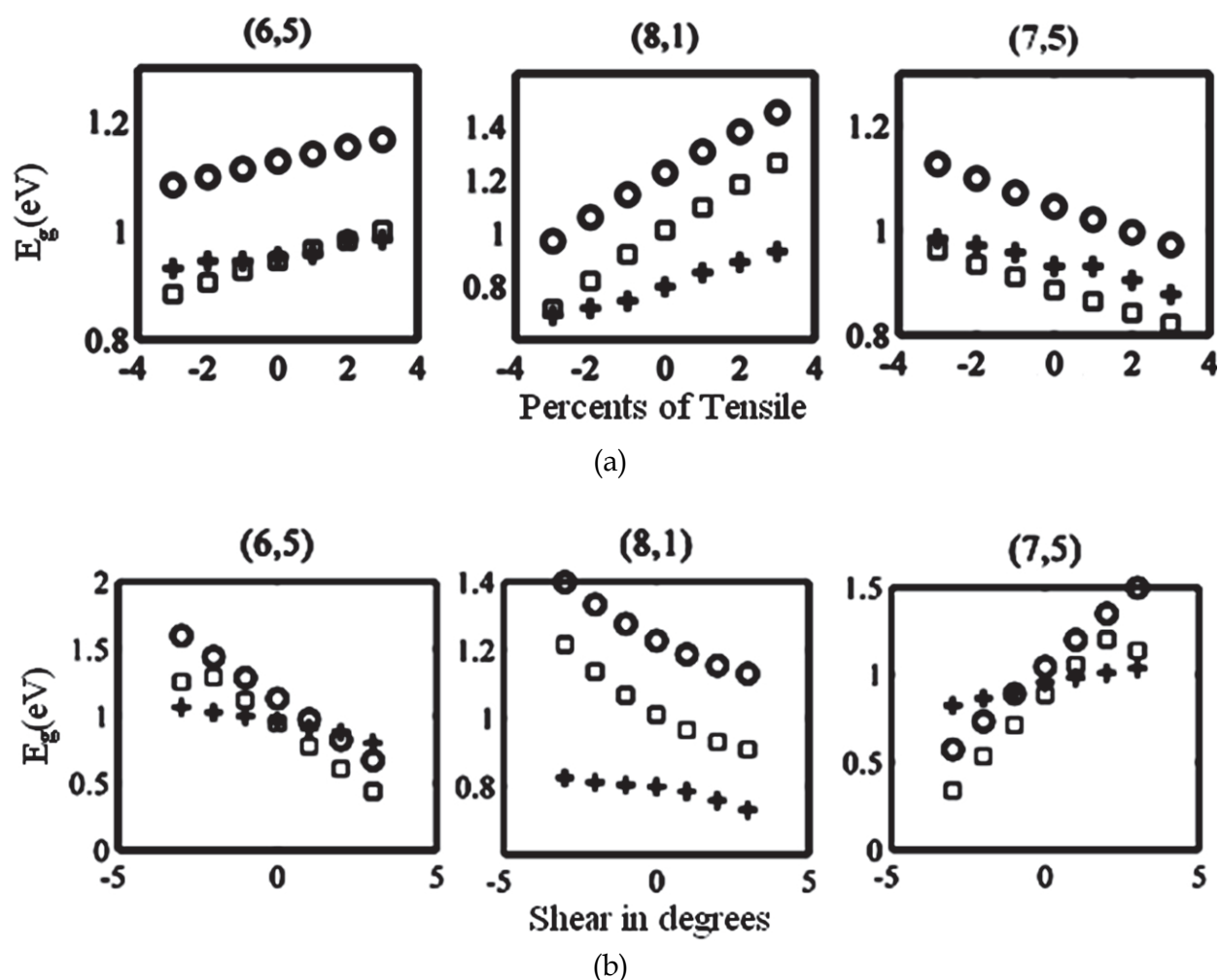

Fig. 8. A comparison between the results obtained using the nearest neighbor π-TB (circles), the third neighbor π-TB (squares), four orbital TB (plus signs) for (a) -3 to +3 percents of uniaxial strain (b) -3 to +3 degrees of shear [15].

As shown in Fig. 8 the method is examined for three chiral vectors, namely (6,5), (8,1) and (7,5). It can roughly be seen that, the 3rd neighbor π-TB approach yields a better agreement with the four orbital TB than the nearest neighbor π-TB. If we examine the energy formulae for a wide variety of chiral vectors, we find that, there is an approximately, linear relation between the percents of strain (both uniaxial and torsional) and the increase in band-gap [15].

4.2 The investigation of the band structure under magnetic field

The effect of magnetic field on the electronic band structure of SWCNT is the second effect that is investigated in this section. The application of H field parallel to the tubule axis is investigated by $k.p$ method in [16],[17] and an Aharanov-Bohm effect is shown during this investigation. In this section the effect of perpendicular magnetic field is investigated using π-TB model. The investigation is originally performed by R. Saito et al. [18]. The investigation is based on two assumptions: first, the atomic wave function is localized at a carbon site; second, the magnetic field varies sufficiently slowly over a length scale equal to the lattice constant. The vector potential $\mathbf{A}$ is declared as:

$$\mathbf{A} = (0, \frac{LH_M}{2\pi}\sin\frac{2\pi}{L}x) \tag{45}$$

where L = $|\mathbf{C}|$, H_M is the magnetic field and the coordinates x and y are taken along the circumference and the axis of the nanotube, respectively. Under the perpendicular magnetic field the basis functions of (30-a) and (30-b) are changed to:

$$\left|\varphi_s\right\rangle = \frac{1}{\sqrt{N_t}} \sum_{Lattice} e^{i(\mathbf{k}.\mathbf{R}_s + \frac{e}{\hbar c}G_\mathbf{R})} \chi_\mathbf{r}(\mathbf{r} - \mathbf{R}_s) \qquad s = A,B \tag{46}$$

$G_\mathbf{R}$ is the phase factor that is associated with the magnetic field and is expressed as the following:

$$G_\mathbf{R} = \int_\mathbf{R}^\mathbf{r} \mathbf{A}(\xi).d\xi = \int_0^1 (\mathbf{r} - \mathbf{R}).\mathbf{A}[\mathbf{R} + \lambda(\mathbf{r} - \mathbf{R})]d\lambda \tag{47}$$

Under application of magnetic field Hamiltonian operator becomes:

$$H = \left(\frac{1}{2m}\right)\left[\mathbf{p} - \frac{e}{c}\mathbf{A}\right]^2 + V \tag{48}$$

After application of Hamiltonian to (46):

$$H\left|\varphi_s\right\rangle = \frac{1}{\sqrt{N_t}} \sum_{Lattice} e^{i(\mathbf{k}.\mathbf{R}_s + \frac{e}{\hbar c}G_\mathbf{R})} \left\{\left(\frac{1}{2m}\right)\left[\mathbf{p} - \frac{e}{c}\mathbf{A}\right]^2 + V\right\} \chi_\mathbf{r}(\mathbf{r} - \mathbf{R}_s) \tag{49}$$

Since $\mathbf{B} = \nabla \times \mathbf{A} = \nabla \times (\mathbf{A} - \nabla G_\mathbf{R})$ and considering (47), then:

$$H|\varphi_s\rangle = \frac{1}{\sqrt{N_t}} \sum_{Lattice} e^{i(\mathbf{k}.\mathbf{R}_s + \frac{e}{\hbar c}G_\mathbf{R})} \left\{ \left(\frac{1}{2m}\right)\left[\mathbf{p} - \frac{e}{c}(\mathbf{A} - \nabla G_\mathbf{R})\right]^2 + V \right\} \chi_\mathbf{r}(\mathbf{r} - \mathbf{R}_s) =$$

$$\frac{1}{\sqrt{N_t}} \sum_{Lattice} e^{i(\mathbf{k}.\mathbf{R}_s + \frac{e}{\hbar c}G_\mathbf{R})} \left(\frac{\mathbf{p}^2}{2m} + V\right) \chi_\mathbf{r}(\mathbf{r} - \mathbf{R}_s) \qquad (50)$$

In deriving the equation above the two mentioned assumptions are used, namely, it is assumed that the magnetic field is slowly changing compared with the change of $\chi_r(\mathbf{r} - \mathbf{R}_s)$ and $\chi_r(\mathbf{r} - \mathbf{R_s})$ is localized at $\mathbf{r} = \mathbf{R_s}$. Now, we can calculate the matrix elements of Hamiltonian between the two Bloch functions, $|\varphi_1\rangle$ and $|\varphi_2\rangle$ and solve to obtain the eigenvalues. If we examine the п-TB calculated band structure, it is observed that when the magnetic field increases the energy dispersion of each tubule energy band becomes narrower and the total energy bandwidth decreases with increasing magnetic field ,however, when we apply higher magnetic field the total energy bandwidth is found to oscillate as function of H_M [18].

5. Conclusion

In this chapter we first described the concept of chiral vector, chiral angle and the radius of SWCNTs and formulated them. Then we explained different symmetries of single walled carbon nanotubes including translational, helical and rotational symmetries. We investigated the Brillouin zone and the electronic band structure of single walled carbon nanotube in the absence of perturbating mechanisms. Our investigation included the nearest neighbor п-TB and the third nearest neighbor п-TB approximations. Next, using these two models we investigated the effect of two types of mechanical strain and perpendicular magnetic field.

6. References

[1] S. Iijima, Nature (London) Vol. 354, pp. 56-58, (1991)
[2] R. Saito, M. Fujita, G. Dresselhaus, M. S. Dresselhaus, Appl. Phys. Lett. 60, 2204 (1992)
[3] V. N. Popov, L. Henrard. Phys. Rev. B 70. 115407(2004)
[4] L. Yang , M. P. Anantram, J. Han, J. P. Lu, Phys. Rev. B 60,13874 (1999)
[5] M. Pakkhesal, R. Ghayour, Cent. Eur. Phys. 6, 824 (2008)
[6] M. Pakkhesal, R. Ghayour, Z. Kordrostami, Fullerenes, Nanotubes and Carbon Nanostructures, 17, 99 (2009)
[7] C. T. White, D.H. Robertson, J. W. Mintmire. Phys. Rev. B 47. 5485 (1993)
[8] Kittel, "Solid State Physics", (1999)
[9] R. Saito, M. Fujita, G. Dresselhaus, M. S. Dresselhaus. Phys. Rev. B 46. 1804(1992)
[10] P.R. Wallace Phys. Rev. 71 (1947)
[11] S. Reich, C. Thomsen. Phys. Rev. B 65 .15541(2002)
[12] J. W. Mintmire, B.I. Dunlap, C. T. White. Phys. Rev. B 63. 073408 (1993)
[13] S. Reich, C. Thomsen. Phys. Rev. B 65 .15541(2002)

[14] L. Yang, M. P. Anantram, J. Han, J. P. Lu, Phys. Rev. B, 60, 13874, 1999

[15] M. Pakkhesal, R. Ghayour, Cent. Eur. Phys. 8, 304 (2010)

[16] H. Ajiki, T. Ando, J. Phys. Soc. Jpn 62, 1255 (1993)

[17] H. Ajiki, T. Ando, J. Phys. Soc. Jpn. 62, 2470 (1993)

[18] R. Saito, G. Dresselhaus, M. S. Dresselhaus. Phys. Rev. B 50.
      14698 (1994)
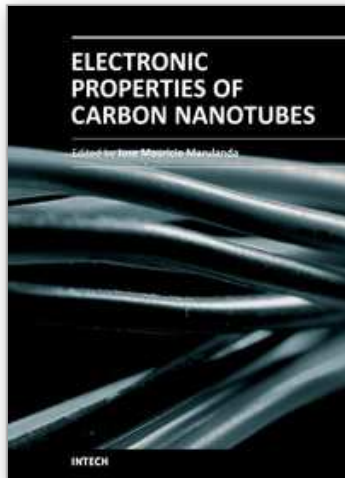
Electronic Properties of Carbon Nanotubes

Edited by Prof. Jose Mauricio Marulanda

Carbon nanotubes (CNTs), discovered in 1991, have been a subject of intensive research for a wide range of applications. These one-dimensional (1D) graphene sheets rolled into a tubular form have been the target of many researchers around the world. This book concentrates on the semiconductor physics of carbon nanotubes, it brings unique insight into the phenomena encountered in the electronic structure when operating with carbon nanotubes. This book also presents to reader useful information on the fabrication and applications of these outstanding materials. The main objective of this book is to give in-depth understanding of the physics and electronic structure of carbon nanotubes. Readers of this book should have a strong background on physical electronics and semiconductor device physics. This book first discusses fabrication techniques followed by an analysis on the physical properties of carbon nanotubes, including density of states and electronic structures. Ultimately, the book pursues a significant amount of work in the industry applications of carbon nanotubes.

How to reference

In order to correctly reference this scholarly work, feel free to copy and paste the following:

Rahim Ghayour and Pakkhesal (2011). Electronic Band Structure of Carbon Nanotubes in Equilibrium and None-Equilibrium Regimes, Electronic Properties of Carbon Nanotubes, Prof. Jose Mauricio Marulanda (Ed.), ISBN: 978-953-307-499-3, InTech, Available from: http://www.intechopen.com/books/electronic-properties-of-carbon-nanotubes/electronic-band-structure-of-carbon-nanotubes-in-equilibrium-and-none-equilibrium-regimes

INTECH
open science | open minds